

Time-resolved optical mammography using a liquid coupled interface

Tara D. Yates

Jeremy C. Hebden

Adam P. Gibson

Louise Enfield

Nicholas L. Everdell

University College London
Department of Medical Physics & Bioengineering
London WC1E 6BT
United Kingdom

Simon R. Arridge

University College London
Department of Computer Science
London WC1E 6BT
United Kingdom

David T. Delpy

University College London
Department of Medical Physics & Bioengineering
London WC1E 6BT
United Kingdom

Abstract. A method has been devised for generating three-dimensional optical images of the breast using a 32-channel time-resolved system and a liquid-coupled interface. The breast is placed in a hemispherical cup surrounded by sources and detectors, and the remaining space is filled with a fluid with tissue-like optical properties. This approach has three significant benefits. First, cups can accommodate a large range of breast sizes, enabling the entire volume of the breast to be sampled. Second, the coupling of the source and detector optics at the surface is constant and independent of the subject, enabling intensity measurements to be employed in the image reconstruction. Third, the external geometry of the reconstructed volume is known exactly. Images of isolated targets with contrasting absorbing and scattering properties have been acquired, and the performance of the system has been evaluated in terms of the contrast, spatial resolution, and localization accuracy. These parameters were strongly dependent on the location of the targets within the imaged volume. Preliminary images of a healthy human subject are also presented, which reveal subtle heterogeneity, particularly in the distribution of scatter. The ability to detect an absorbing target adjacent to the breast is also demonstrated. © 2005 Society of Photo-Optical Instrumentation Engineers. [DOI: 10.1117/1.2063327]

Keywords: near-infrared imaging; breast imaging; optical tomography.

Paper 04189R received Oct. 1, 2004; revised manuscript received Apr. 20, 2005; accepted for publication May 18, 2005; published online Oct. 4, 2005.

1 Introduction

Breast cancer is the second leading cause of cancer deaths in women. According to the World Health Organization, more than 1 million women worldwide were diagnosed with breast cancer in 2000.¹ However, it has been shown that early detection and diagnosis of the disease significantly reduces the mortality rate and also the need for more extensive surgery.² The principal imaging modality used in breast imaging at present is x-ray mammography which, while it has a high sensitivity, suffers from a relatively poor specificity for some tumors and breast types, leading to unnecessary biopsies.³ Thus there is a need for alternative imaging techniques that can noninvasively distinguish between malignant and benign lesions, particularly in the younger, denser breast. At present both magnetic resonance imaging (MRI) and ultrasound are used to provide additional diagnostic information for this purpose. The disadvantages of MRI are that a contrast agent is generally required, it is immobile, and it is expensive.⁴ Ultrasound, while relatively inexpensive and versatile, is dependent on operator expertise and provides relatively poor distinction between certain solid breast masses.⁵

Optical tomography provides a distinction between tissues based on their optical properties obtained from measurements

of transmitted light.⁶ Of particular interest is the facility to exploit the differences between the absorption spectra of oxy-hemoglobin and deoxy-hemoglobin at near-infrared wavelengths to produce images of blood volume and oxygen saturation.^{7,8} It is anticipated that this physiological information can add to the anatomical information gained from x-ray mammography to produce a better diagnosis.^{9,10}

The use of optical radiation to image the breast is not a new concept, and interest in the subject first became widespread in the mid-1980s. This was stimulated by the emergence of new source and detector technologies¹¹ along with substantial developments in computing technology, allowing the use of sophisticated algorithms to reconstruct images representing the optical properties contained within a three-dimensional (3D) volume.^{12,13} Since then, many researchers have built, and begun clinical evaluations of, breast imaging systems that exploit one or both of these developments. Some groups¹⁴⁻¹⁶ have developed optical tomography systems which acquire measurements of transmitted intensity. Other groups¹⁷⁻²² have followed a more technically complex approach using time and frequency domain systems to measure the characteristic response of breast tissues to illumination by pulsed and intensity modulated sources, respectively. Development of these systems has been motivated in part by the inability of intensity measurements alone to yield separate images of internal absorbing and scattering properties of

Address all correspondence to Adam Gibson, University College London, Department of Medical Physics and Bioengineering, Malet Place Engineering Building-Gower Street, London, WC1E 6BT United Kingdom. Tel.: 44-20-7679-0279; Fax: 44-20-7679-0255; E-mail: agibson@medphys.ucl.ac.uk

tissue,²³ unless additional (e.g., spectral) information is available.

One of the inherent challenges of so-called optical mammography is to develop means of coupling appropriate sources and detectors to the breast. This problem is by no means trivial and various mechanisms have been explored. Some groups^{9,24,25} use a compressed breast geometry, where one or more sources and detectors are scanned over both surfaces and a single projection image analogous to an x-ray mammogram is generated. A specific disadvantage of a compression technique is that prolonged compression can produce significant discomfort.²⁶ An alternative method is to surround the breast with a rigid circular array of sources and detectors and reconstruct either a cross-sectional slice or the whole volume.²⁷⁻²⁹ At University College London (UCL) we initially evaluated an interface consisting of two rings of different sizes, to which the sources and detectors were attached, mounted on a frame.^{29,30} The breast was placed into whichever ring provided the better fit for that patient. However, this approach also has its limitations: a rigid ring cannot conform to the shape of the breast, and it is difficult to sample the entire breast volume so that lesions (near the chest wall, for example) are not missed. A further potential disadvantage of all methods involving placing sources and detectors in direct contact with the breast is that the coupling of light into and out of the breast is usually highly variable, which reduces the reproducibility with which intensity measurements can be achieved.³⁰ An approach which overcomes most of these problems is that originally adopted by Colak et al.²⁸ at Philips Research Laboratories, who used a container filled with a tissue-matching fluid. This has three significant benefits. First, the container can be made of a sufficient size to accommodate a large range of breast sizes and shapes, enabling the entire 3D volume of the breast to be sampled. Second, the coupling of the source and detector optics at the surface is constant and independent of the subject. And third, the external geometry of the reconstructed volume is known exactly, so an accurate model can be generated.

As described in the following section, optical tomography at UCL is based on a 32-channel time-resolved system. We have recently developed a liquid-coupled interface suitable for breast imaging based on a hemispherical cup. The cup has a diameter of 165 mm, which was estimated to be sufficiently large for the majority of women undergoing x-ray mammography at UCL. The cup volume is significantly larger than that reconstructed for most previous optical tomography applications, and this is expected to have an impact on the ability to detect small and/or low-contrast features. Therefore, before beginning a program of clinical tests on a variety of human volunteers and patients, we performed a thorough evaluation of the overall imaging performance. Specifically, we determined the spatial resolution, contrast, and localization accuracy likely to be achieved with the system, and the results of the study are presented here. The outcomes of this study will enable the results of later clinical studies to be validated, and will hopefully lead to improved methods of deriving quantitative information.

2 Method

2.1 The UCL Optical Tomography System

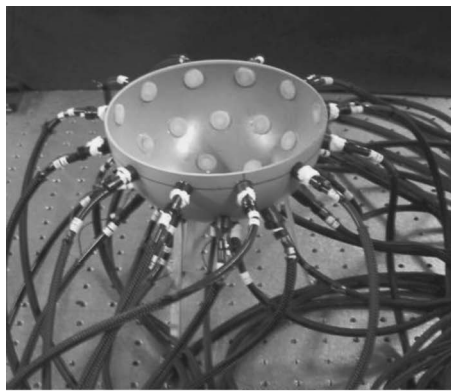
A 32-channel time resolved system for optical tomography developed at UCL has been described in depth elsewhere.²² It consists of a portable fiber laser (IMRA Inc., USA) that produces pulses ~ 2 ps in duration at 780 nm and 815 nm, interleaved with an overall repetition rate of 80 MHz. These pulses are transmitted through a 32-way optical switch that illuminates each source fiber in sequence. Each source fiber is integrated along the axis of a detector fiber bundle. Combining the sources and detectors in this way reduces the number of connection points on the tissue being imaged, and facilitates a straightforward method of calibrating the temporal characteristics of the system.³¹ The detector fiber bundles collect the light that has traveled through the breast and transmit it to four 8-anode microchannel-plate photomultiplier tubes (MCP-PMTs). The MCP-PMTs produce an electronic pulse for each photon detected and are protected from over exposure by a series of programmable variable optical attenuators.

The detector electronics consists of 32 parallel channels which measure the times taken for photons to travel between each source and detector relative to a reference pulse generated by the laser, and produce a series of time-of-flight histograms known as temporal point spread functions (TPSFs). Datatypes such as integrated intensity, mean flight time, and temporal variance are typically extracted from the measured TPSFs. The use of such datatypes decreases the computational time and memory requirements of the reconstruction algorithm as compared to calculating the entire TPSF. Intensity and meantime were used here as these have proved to be the most robust and the most effective at separating scatter and absorption.³²

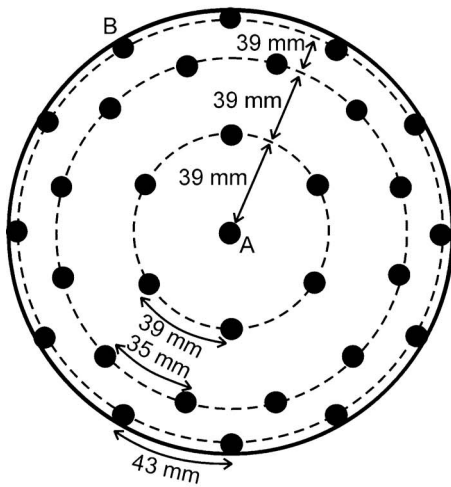
2.2 The Liquid-Coupling Interface

The coaxial source/detector bundles are attached to the exterior of an opaque plastic hemispherical cup, 165 mm in diameter with a thickness of 5 mm (EMA model supplies, Shepperton, UK). Thirty-one bundles are distributed over the surface of the cup as illustrated in Figs. 1(a) and 1(b). The bundles are spaced at regular intervals within three horizontal planes, providing a reasonably even distribution across the surface of the hemisphere. Holes were drilled in the opaque cup, and optically scattering windows were attached to the inner surface to form a watertight seal across each hole. Each window was made from a mixture of epoxy resin and titanium dioxide particles, providing highly scattering properties to create a diffuse source.³³ The fiber bundles are held in position using short plastic tubes attached to the external surface of the cup.

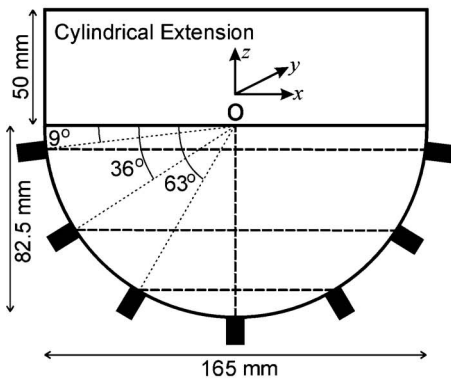
The remaining space between the breast and the cup is filled with a suitable coupling liquid. In the study performed with a similar device by the Philips group,²⁸ the optical properties of the coupling fluid were selected to match the average optical properties of the breast. This offers two obvious advantages. First, the reconstruction algorithm is not required to iterate too far from a uniform initial guess corresponding to those average optical properties, and is therefore more likely to converge to a correct solution. Second, contrast in the reconstructed images will be dominated by the features of interest within the breast, instead of by the differences between



(a)



(b)



(c)

Fig. 1 The hemispherical cup developed for breast imaging: (a) a photograph showing 31 fiber bundles attached; (b) the arrangement of sources/detectors as seen from above; (c) a side view of the cup and the vertical extension used for reference measurements.

the breast and fluid properties. A further consideration is that the coupling fluid must be harmless to skin contact. For the purposes of this preliminary investigation the cup was filled with a solution of intralipid,³⁴ dye, and distilled water with properties of absorption coefficient $\mu_a = 0.0070 \pm 0.00035 \text{ mm}^{-1}$ and reduced scattering coefficient $\mu'_s = 0.80 \pm 0.04 \text{ mm}^{-1}$. These values were chosen as being

representative of the average properties of the breast^{35,36} and are consistent with those used in previous breast phantom studies at UCL.³⁷ These properties also ensured that the signal acquired for the largest source-detector separation (corresponding to the full diameter of 165 mm) produced a measured photon count rate of around 50 to 100 photons per second, sufficient to obtain useful datatypes for image reconstruction.

Throughout this study a so-called difference imaging approach was performed. Difference imaging involves reconstructing the changes in optical properties between the cup containing both the coupling fluid and the breast, and those of a suitable reference medium. The advantage of using difference imaging as opposed to absolute imaging is that systematic errors inherent in the measurement largely cancel. For this application, difference imaging eliminates the effect of uncertainty and variability in the surface coupling, allowing use of intensity measurements. Disconnecting and reconnecting the fiber bundles to the cup has shown that the coupling can vary, and therefore absolute imaging would require the coupling to be measured empirically for each scanning session. The disadvantage of difference imaging is that errors will occur if the reference medium is poorly matched to the breast and its properties are not known exactly.³² The ideal reference is a homogeneous medium with known optical properties and external geometry, which are the same as the object under investigation. Such a reference can be created for this system by filling the cup with the coupling fluid described above.

Initial experiments with the cup revealed that measurements recorded with sources and detectors located near to the top of the hemisphere are highly sensitive to the proximity of the top surface of the liquid.³⁸ Furthermore, to provide a reasonable reference for patient studies (since detected photons can travel into and out of the chest wall) it is necessary to extend the height of the reference medium. Various alternative methods of extending the height have been explored.³⁸ The two most successful are the addition of an extra volume of coupling liquid, and the use of a solid cylindrical slab of tissue-equivalent phantom material placed in contact with the top surface of the liquid. The former was achieved by attaching a cylindrical plastic extension, 50 mm in height, to the top of the hemisphere as illustrated in Fig. 1(c). The height of liquid necessary to avoid significant loss of detected light from the top surface was established empirically.³⁸ The disadvantages of this method are that it requires several additional minutes to attach and fill the plastic extension, and it is difficult to maintain a reusable watertight seal. The cylindrical block was made from epoxy resin with a diameter of 200 mm and a thickness of 65 mm. The optical properties of the block are $\mu_a = 0.007 \text{ mm}^{-1}$ and $\mu'_s = 2.0 \text{ mm}^{-1}$. The scatter coefficient was chosen to represent the anticipated higher scattering within the chest wall, such as due to bone. The cylindrical block method is much easier to employ, although there is a concern how a mismatch in refractive index between the resin block (1.56) and the coupling fluid (1.33) may affect the reconstruction.³⁹

The repetition rate of the laser (two interlaced trains of pulses at 40 MHz) dictates that the maximum temporal window for each TPSF is 12.5 ns. However, the large diameter of

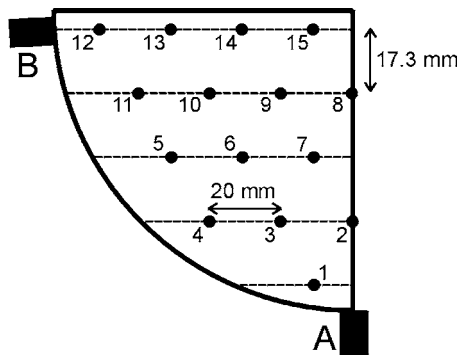


Fig. 2 The positions of the targets within a half-plane of the cup.

the cup and the optical properties of the coupling fluid cause some photons for the largest source-detector separations to be detected with flight times in excess of the window width. As a consequence it is necessary to acquire data at the two wavelengths successively rather than simultaneously, enabling a temporal window of 25 ns to be used. In the experiments reported below, data were only acquired at a single wavelength of 815 nm.

2.3 Perturbation Experiments

To quantify the spatial resolution, localization accuracy, and contrast across the volume of the cup, two epoxy resin cylindrical targets with length and diameter of 10 mm were constructed. The optical properties of these are as follows. Target A: $\mu_a=0.07 \text{ mm}^{-1}$ ($10 \times$ background μ_a) and $\mu'_s=0.8 \text{ mm}^{-1}$, and target S: $\mu_a=0.007 \text{ mm}^{-1}$ and $\mu'_s=8 \text{ mm}^{-1}$ ($10 \times$ background μ'_s), respectively. The targets were each placed at 15 positions within one half-plane of the fluid filled cup as illustrated in Fig. 2. These positions form a grid of equilateral triangles.

Each target was suspended in turn on the end of a thin wire supported by a frame mounted on vertical and horizontal translation stages. The target was initially placed in the center of the top ring of fiber bundles and was translated relative to this point. Data were acquired for 11 min at each position with an acquisition time of 10 s per source. Reference data sets were acquired with the target removed at the end of each row in Fig. 2, as well as prior to and following the experiment.

2.4 Patient Interface

A patient-supporting table was built to enable the system to be evaluated on volunteers. The cup is attached to a plastic ring secured firmly into an aperture in the table as illustrated in Fig. 3. A channel is cut into the ring, which allows coupling fluid that overflows from the cup to return via plastic tubing to the fluid reservoir. The cup is filled with fluid from below using a peristaltic pump, which then circulates fluid continuously and slowly to sustain a constant level of fluid. The addition of a heating element to the fluid reservoir will ultimately enable the liquid to be maintained at a constant, comfortable temperature. The table is covered with a layer of foam, and a pillow and towels are provided.

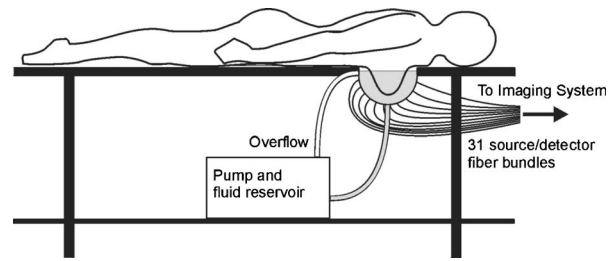


Fig. 3 A schematic of the breast imaging table and liquid-circulating mechanism.

2.5 Preliminary Studies on Healthy Volunteers

Initial studies have been performed on several healthy volunteers. Prior to the investigation, the coupling fluid was prepared at an ambient room temperature of 23°C. Data were acquired on each of the volunteer's breasts for a total scan time of 11 min, or 10 s per source. To enable difference measurements to be used in the reconstruction, two different references were used and compared. One volunteer was also scanned a second time with the high-absorbing target (described above in Sec. 2.3) attached to the surface of her breast with Micropore (3M) paper tape.

2.6 Image Reconstruction

Images were generated from the data using the TOAST reconstruction package developed at UCL.⁴⁰ TOAST employs the finite element method (FEM) to model the propagation of light through tissue using the diffusion approximation to the radiative transfer equation. TOAST reconstructs 3D images of scatter and absorption coefficients. Image reconstruction involves iteratively adjusting the optical properties assigned to the FEM mesh to optimize the match of the model to the data.

A 3D finite element mesh was constructed with a Delaunay triangulation method to be used in reconstruction of the data obtained using the hemispherical cup.⁴¹ The mesh, shown in Fig. 4, was generated as a hemisphere with a 50-mm cylindrical extension to the top. The mesh consists of 23,156 tetrahedral elements with quadratic interpolation functions and

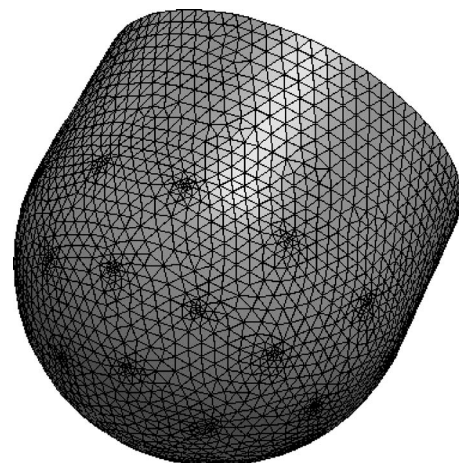


Fig. 4 The finite-element mesh used for image reconstruction.

35,233 nodes. The mesh has a greater density at the positions of the source detector bundles, where the rate of change of light intensity is greater.

The image reconstruction was performed using a conjugate gradient solver and Robin boundary conditions. In all cases, the 15th iteration was analyzed as this was found to be the number beyond which no further improvement to the images was observed. Each iteration required 48 min on a 2.2 GHz Xeon processor and used approximately 800 MB of RAM.

2.7 Analysis

The contrast, spatial resolution, and localization accuracy were determined from images obtained for all the 15 positions indicated in Fig. 2. The contrast C is calculated using:

$$C = \frac{y_{\max} - y_{bg}}{y_{bg}}, \quad (1)$$

where y_{\max} was taken to be the mean of the top 5% of all values in each 3D image and y_{bg} was the mean background value calculated from the remaining data in the image. In other words, no prior knowledge of the position of the target was employed in the calculation of contrast.

The localization accuracy was determined from the differences between the positions of the peak value within the images and the expected positions of the target. The position of the peak value was obtained by taking the mean x , y , and z values for the nodes in the mesh that correspond to values above 95% of the maximum value. Any difference between the expected positions and the true positions (due to error in the initial positioning of the targets) was removed by subtracting the mean expected values and the mean measured values from the corresponding values of x , y , and z . Any difference between the expected and measured values is then only due to the reconstruction error we wish to quantify.

Each 3D image may be considered to represent the target distribution convolved with a 3D point spread function (PSF). It is conventional to characterize spatial resolution in terms of the width of the PSF. For the analysis presented here, however, we elect to characterize spatial resolution in terms of the *volume* of the PSF. Since the volume of the images of the targets are much greater than that of the targets themselves, we make the approximation that the PSF volume is equal to the volume of the reconstructed target. The “volume resolution” presented here has been calculated as the volume of the mesh that encompasses all nodes associated with a value greater than or equal to 50% of the maximum value in the image. We call this parameter the full volume at half maximum (FVHM).

The PSF is assumed to have a Gaussian profile. When the volume occupied by the feature in the image becomes greater, the peak value (and therefore the contrast) will be reduced. Hence a decrease in spatial resolution will lead to a direct decrease in contrast, which can be expressed as:

$$V_t h_t = V_i h_i, \quad (2)$$

where V_t is the true volume of the target, V_i is the volume of the feature in the image, and h_t and h_i are the values of $y_{\max} - y_{bg}$ for the target and the image, respectively. Thus, assuming the background y_{bg} of the image to be equal to the

true background of the medium, we can express the apparent contrast of the target by:

$$C_i = C_t \frac{V_t}{V_i}, \quad (3)$$

where C_t is the true contrast of the target. Thus in principle, we should be able to compensate for the reduction in contrast due to the size of the PSF by multiplying the apparent contrast by a factor equal to V_i/V_t . We can estimate V_i from the calculated value of the FVHM by assuming it to be a 3D Gaussian. The equation for a Gaussian is given by:

$$y(r) = h e^{-r^2/2\sigma^2}, \quad (4)$$

where σ is the standard deviation, h is the amplitude of the Gaussian, and r is the distance from the center of the distribution. The volume of the 3D Gaussian (V_g) can be obtained from integration of Eq. (4):

$$V_g = h(\sqrt{2\pi}\sigma)^3. \quad (5)$$

By defining a full width at half maximum f such that $y(f/2) = h/2$ we obtain:

$$\sigma = \frac{f}{\sqrt{8 \ln 2}}. \quad (6)$$

Substituting Eq. (6) into Eq. (5) then gives:

$$V_g = h \left(\frac{\pi}{4 \ln 2} \right)^{3/2} f^3. \quad (7)$$

However, our measured value of FVHM represents a sphere of radius $f/2$, which implies that:

$$f^3 = \frac{6}{\pi} FVHM. \quad (8)$$

By combining Eqs. (7) and (8) we obtain:

$$V_g = h \left(\frac{\pi}{4 \ln 2} \right)^{3/2} \frac{6}{\pi} FVHM \approx 2.3 h FVHM. \quad (9)$$

Thus V_i can be estimated from the FVHM by multiplying by a factor of 2.3.

3 Results

3.1 Perturbation Experiments

Figure 5 shows typical images reconstructed from the data acquired for the (a) absorbing and (b) scattering targets in position 11 in Fig. 2. These images represent x - z and x - y slices [see Fig. 1(c)] through the 3D images, intersecting the peak produced by the target. In each case the 15th iteration is shown. Although the targets are displayed in the expected location, we observe significant crosstalk between absorption and scatter. The TOAST algorithm has interpreted the difference data for both types of target as a perturbation in both parameters, although the largest perturbation is identified in the correct parameter (see discussion in Sec. 4).

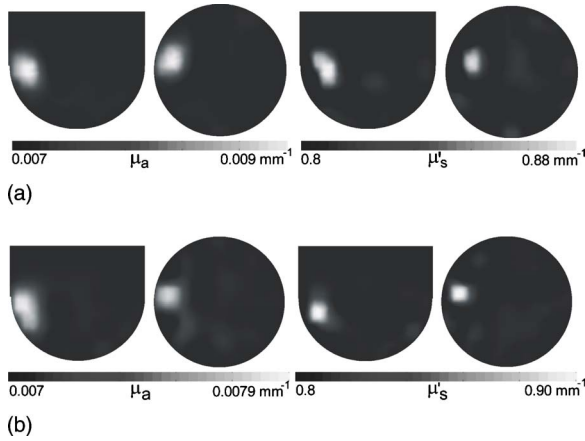
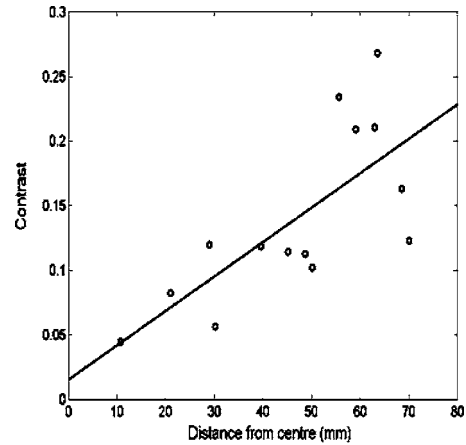


Fig. 5 The reconstructed absorption (left) and scattering (right) images of (a) absorbing target A placed at position 11, and (b) scattering target S at position 11.

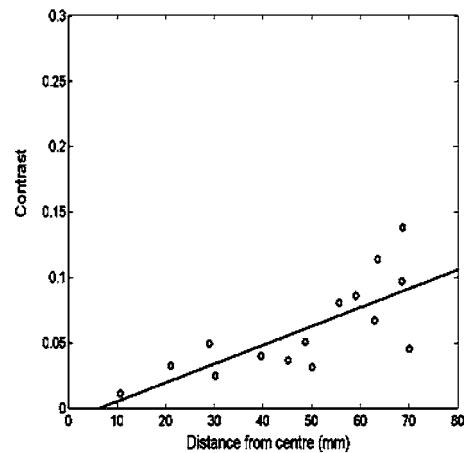
Plots of the variation in contrast, localization accuracy, and FVHM (as defined in Sec. 2.7) with distance from the coordinate origin [position O in Fig. 1(c)] are shown in Figs. 6, 7, and 8, respectively. A linear trend line was fitted to each set of data using a least-squares regression. All three plots show strong dependency on the position of the cylinder from the edge of the cup. A plot of the adjusted contrast ($V_i C_i / V_i$) against distance from the coordinate origin is shown in Fig. 9. As discussed in Sec. 4 below, the values obtained are significantly closer to the true contrast of 9, suggesting that such a method could be useful for improving the quantitation accuracy of optical tomography.

3.2 Initial Images Using the System on a Healthy Volunteer

The reconstructed absorption and scatter images of a 69-year-old healthy volunteer's left breast are shown in Fig. 10(a). In this case, the reference data was acquired using the additional height of coupling fluid. Reassuringly, an image acquired using the solid resin block on the top surface of the cup (not shown) was almost identical, both qualitatively and quantitatively, despite the refractive index mismatch for the resin block. The absorption and scatter images both exhibit reasonable contrast, although the scatter images generally show greater heterogeneity. Meanwhile, Fig. 10(b) shows the images of the same breast with the absorbing target attached to the surface of the breast (near position 5 in Fig. 2). The vertical (x - z) and horizontal (x - y) slices in Fig. 10(b) correspond to the planes through the apparent center of the absorbing target, and the same planes are selected for Fig. 10(a). The contrast of the target (in both absorption and scatter images) is entirely consistent with that shown for the isolated target in a similar position in Fig. 5(a). Allowing for some slight movement of the breast between the two measurements, the appearance of the breast in Fig. 10(b) is very similar to that shown in Fig. 10(a). The uncertainty in the nominal optical properties of the coupling fluid is roughly 5%, so the boundary between the breast and fluid is difficult to determine in terms of optical properties alone. Nevertheless, the images suggest that while the breast is generally more absorbing than the fluid, the



(a)



(b)

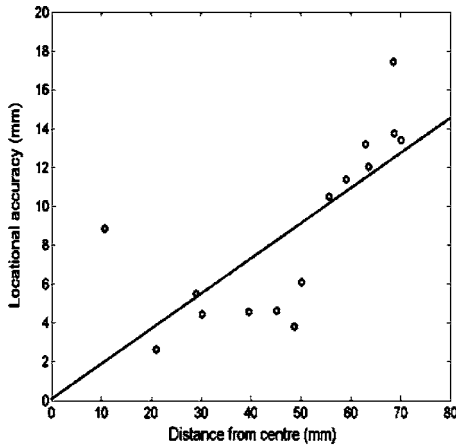
Fig. 6 The contrast of (a) target A and (b) target S plotted against distance from the center of the cup (using the 15th iteration).

breast contains regions which are evidently less scattering than the fluid. This may be indicative of regions of adipose tissue, which is expected to be lower scattering than other tissues and more dominant in the older, postmenopausal breast.⁴²

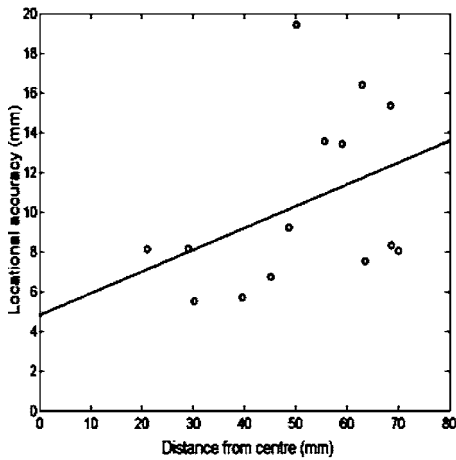
4 Discussion

The use of the coupling fluid in the manner described above has enabled both intensity and meantime difference measurements to be used to reconstruct 3D images for both absorption and scatter. This represented a major advance upon our earlier breast imaging studies at UCL where intensity was unavailable due to inconsistent coupling between the breast and the fiber bundles.^{29,30} This technique also has the advantage that a simple generic mesh can be used in the reconstruction, avoiding the necessity to generate a patient-specific mesh for each study.

The spatial resolution, presented here as a value of FVHM (Fig. 8), decreases from 60 to 6 cm^3 for target A, and from 30 to 5 cm^3 for target S, as they approach the edge of the cup. Whereas, in an ideal imaging system, the FVHM would be equal to the true volume of the target (0.8 cm^3) and be independent of position, results show that the mean FVHM is



(a)

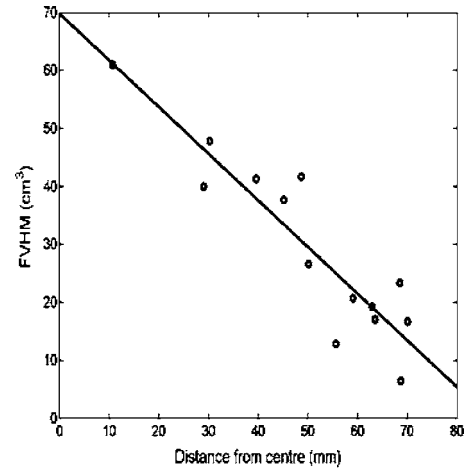


(b)

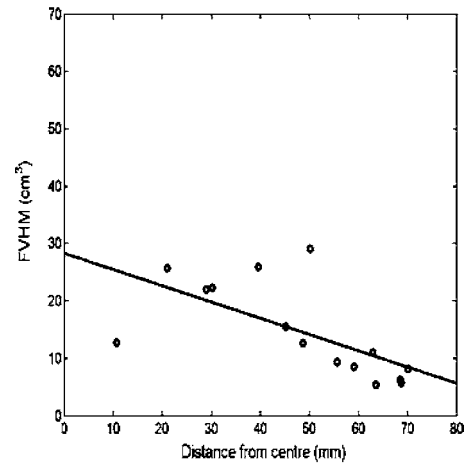
Fig. 7 The localization accuracy for (a) target A and (b) target S plotted against distance from the center of the cup (using the 15th iteration).

substantially higher than the true volume, and the FVHM varies by up to a factor of 10. Large source-detector separations (up to 165 mm) result in an inherently lower spatial resolution due to their broad sensitivity functions. Information about the center of the cup is derived only from measurements recorded with the largest source-detector separations, and consequently the spatial resolution is lower toward the center of the cup. The obvious impact of this on imaging the breast is that superficial lesions will be easier to see than deeper ones.

The contrast across the cup for target A exhibits an upward trend from 0.045, close to the center of the cup, to 0.27 at the edge (Fig. 6). A similar trend is seen for target S with a contrast range from 0.011 to 0.14. The true contrast, as defined by Eq. (1), of a target with optical properties of 10 times the background properties would be 9, and of course is independent of position. Overall we observe a much lower contrast than the true contrast throughout the volume, although it generally improves as the target moves away from the center. Underestimation of contrast is largely due to the partial volume effect caused by limited spatial resolution. In theory, we can compensate for this effect by using a multiplication factor of $(2.3FVHM/V_t)$ as described in Sec. 2.7. The results of this



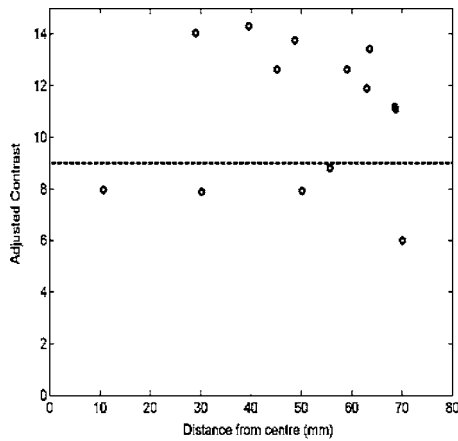
(a)



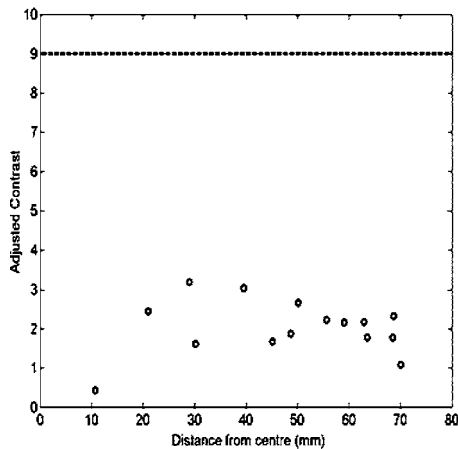
(b)

Fig. 8 The full volume at half maximum for (a) target A and (b) target S plotted against distance from the center of the cup (using the 15th iteration).

method of compensation are presented in Fig. 9, which shows mean values of absorption and scatter contrast of 11.0 and 2.03, respectively. An inevitable cause of the discrepancy between the mean adjusted contrast values (11.0 and 2.3) and the true contrast (9.0) is the crosstalk described earlier in Sec. 3.1. In general, we observe better separation between parameters for absorbing targets than for scattering targets, which is consistent with the larger discrepancy in the adjusted contrast observed for the scattering target. An analysis of the images in Fig. 5, for example, reveals that the absorption contrast is nearly three times higher than the scatter contrast for the absorbing target, while the absorption contrast is roughly equal to the scatter contrast for the scattering target. Furthermore, the graph in Fig. 9 illustrates that the adjusted contrast values showed no clear dependence on the target position. The assumption that the profile of the PSF can be represented by a Gaussian and the arbitrary selection of 50% threshold to define target image volume may also contribute toward a discrepancy between the true and adjusted values of contrast.



(a)



(b)

Fig. 9 Values of contrast following compensation for the partial volume effect for (a) target A and (b) target S plotted against distance from the center of the cup. The dashed lines represent the true contrast value.

The error in target localization, as illustrated in Fig. 7, has surprisingly large mean values of 8.7 mm for target A and 11 mm for target S. This error is largely a consequence of the automated method of determining the center of each target image, where no prior knowledge of target position is employed. We note that the peak value in the image (determined by calculating the centroid of the nodes in the mesh with the top 5% of values) does not generally agree well with the center of the feature identified by inspection. We also find that adjusting the threshold for selecting the volume from which the center position is calculated does not significantly reduce the localization error. It is particularly interesting to note that the localization error increases as the target moves away from the center, even though spatial resolution improves. There are two potential contributing factors. First, the region between a given source and detector to which the measurements are sensitive (the banana-shaped “photon measurement density function” or PMDF⁴³) has a cross-section which changes fastest nearest the source and detector. This will inevitably produce an asymmetry in the reconstructed target image. Second, the external region of the hemisphere is more sparsely sampled,

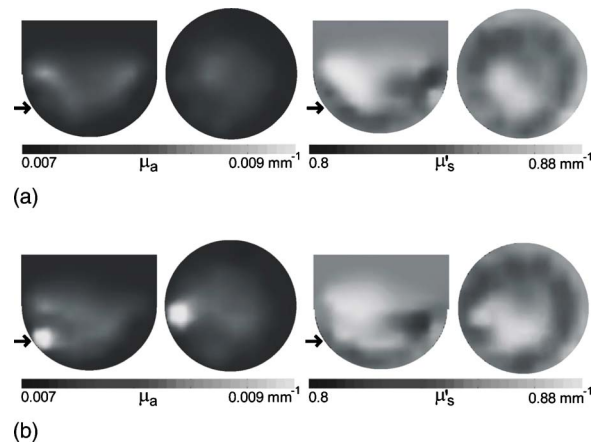


Fig. 10 The reconstructed absorption (left) and scattering (right) images of (a) a healthy 69-year-old volunteer, and (b) the same volunteer with an absorbing target attached to the surface of her breast. The arrows indicate the height of the corresponding circular cross-sections.

and consequently there is likely to be a tendency for the reconstructed targets to be displaced away from their true positions toward the center of the nearest PMDF.

The scatter of values from the linear trends observed in Figs. 6–8 is almost certainly due to the fact that they are plotted against distance from the center of the cup, whereas the values are also influenced by the distances of the targets from individual sources and detectors, sparsely distributed on the surface of the hemisphere. In other words, these parameters are not simply dependent on target depth within the hemisphere, but are actually position-dependent. Although measurements using most of the 31 fiber bundles contribute toward each image, data from the few that are nearest to the target are likely to influence the contrast and spatial resolution most strongly. Unfortunately the distance between a target and the several nearest (and therefore most influential) sources and detectors is not a straightforward quantifiable parameter, and consequently we chose to plot data as a function of distance from the center. In principle, a contrast compensation method could be developed for improving the quantitative accuracy of breast images. However, the method would need to compensate for the effect of convolution between the true distributions of optical properties and the corresponding PSF, which we have shown to be highly position-dependent.

Initial *in vivo* images using this system, shown in Fig. 10, exhibit areas of contrast corresponding to the size and location of the breast. This shows that the inevitable differences between the properties of the coupling solution and the breast can be reconstructed. The area corresponding to the breast itself exhibits a subtle heterogeneity consistent with previous optical tomography studies of healthy volunteers generated using a different patient interface.³⁰ In terms of patient acceptance, we noted that volunteers were very comfortable throughout an 11-min scan, and positioning of the breast within the interface was achieved with more ease than the 2D system employed previously.³⁰

Work is currently in progress to investigate several specific ways of improving the performance of the liquid-coupled system for breast imaging. First, we are producing a range of cup

sizes to ensure optimum sampling of the breast volume using a maximum of 32 source and detector positions. Second, we are investigating the optimum optical properties of the matching fluid. Although matching the properties of the fluid to the mean properties of the breast has certain advantages (outlined in Sec. 2.2), a fluid with a lower attenuation will allow more light to be detected and so may lead to improved image quality. Third, the effect of a change in tissue temperature is being assessed. Slight cooling or heating of the breast by the coupling fluid could lead to blood volume changes during a scan, resulting in image artifacts, although maintaining the fluid at a constant body temperature should prevent this. However, we note that by purposely changing the temperature of the liquid between scans it may be possible to highlight the distribution of blood within the breast (at least near the surface). Finally, our current work is also focused on the utilization of prior information to improve the overall imaging performance. For example, we are investigating whether a measurement of the volume of liquid displaced from the cup by the breast can be employed to constrain the location of the breast boundary (and therefore of the region occupied by the coupling fluid) in the image reconstruction.

In summary, an initial evaluation of a fluid-filled interface for optical tomography of the breast has revealed several major benefits in terms of the ease with which fiber bundles may be coupled to the breast, the availability of intensity data for image reconstruction, the ability to know and model the boundary of the reconstructed volume, and the patient acceptability. We have shown that the contrast and spatial resolution achieved by the technique will be strongly dependent on both the reconstructed parameter and the depth of the tissue. Overall, however, initial results further support the view that the spatial resolution and contrast achievable with optical tomography is unlikely to be sufficient to distinguish diseased from healthy tissues based on morphology alone. Detailed analysis of the spectroscopic content of optical signals are clearly essential in order to obtain the degree of specification required of a clinical diagnostic technique.^{27,44}

Acknowledgments

We thank Dr. Jason Riley for assistance with the data analysis. Support for this work has been generously provided by the Commission for the European Communities (OPTIMAMM) grant (contract QLG1-2000-00690), and by Cancer Research UK.

References

1. J. Ferlay, F. Bray, P. Pisani, and D. M. Parkin, "GLOBOCAN 2000: Cancer Incidence, mortality and prevalence worldwide," Version 1.0. IARC CancerBase No. 5 (2001).
2. L. Tabar L, M.-F. Yen, B. Vitak, H.-H. T. Chen, R. A. Smith, and S. W. Duffy, "Mammography service screening and mortality in breast cancer patients: 20-year follow-up before and after introduction of screening," *Lancet* **361**, 1405–1410 (2003).
3. R. W. Blamey, A. R. M. Wilson, and J. Patnick, "Screening for breast cancer," *BMJ* **321**, 689–693 (2000).
4. M. D. Schnall, "Application of magnetic resonance imaging to early detection of breast cancer," *Breast Cancer Research* **3**, 17–21 (2000).
5. D. D. Pavic, M. D. Koomen, C. D. Kuzmiak, and E. D. Pisano, "Ultrasound in the management of breast disease," *Current Women's Health Rep.* **3**, 156–164 (2003).
6. A. P. Gibson, J. C. Hebden, and S. R. Arridge, "Recent advances in diffuse optical imaging," *Phys. Med. Biol.* **50**, R1–R43 (2005).
7. X. Cheng, J. Mao, R. Bush, D. B. Kopans, R. H. Moore, and M. Chorlton, "Breast cancer detection by mapping hemoglobin concentration and oxygen saturation," *Appl. Opt.* **42**, 6412–6421 (2003).
8. S. Jiang, B. W. Pogue, T. O. McBride, and K. D. Paulsen, "Quantitative analysis of near-infrared tomography: sensitivity to the tissue-simulating precalibration phantom," *J. Biomed. Opt.* **8**, 308–315 (2003).
9. A. Li, E. L. Miller, M. E. Kilmer, T. J. Brukilacchio, T. Chaves, J. Stott, Q. Zhang, T. Wu, M. Chorlton, R. H. Moore, D. B. Kopans, and D. A. Boas, "Tomographic optical breast imaging guided by three-dimensional mammography," *Appl. Opt.* **42**, 5181–5190 (2003).
10. H. Dehghani, B. W. Pogue, S. P. Poplack, and K. D. Paulsen, "Multiwavelength three-dimensional near-infrared tomography of the breast: initial simulation, phantom, and clinical results," *Appl. Opt.* **42**, 135–145 (2003).
11. J. C. Hebden, S. R. Arridge, and D. T. Delpy, "Optical imaging in medicine: I. Experimental techniques," *Phys. Med. Biol.* **42**, 825–840 (1997).
12. S. R. Arridge and J. C. Hebden, "Optical imaging in medicine: II. Modelling and reconstruction," *Phys. Med. Biol.* **42**, 841–853 (1997).
13. S. R. Arridge, "Optical tomography in medical imaging," *Inverse Probl.* **15**, R41–R93 (1999).
14. S. Nioka, Y. Yung, M. Shnall, S. Zhao, S. Orel, C. Xie, B. Chance, and L. Solin, "Optical imaging of breast tumor by means of continuous waves," *Adv. Exp. Med. Biol.* **441**, 227–232 (1997).
15. R. L. Barbour, C. H. Schmitz, D. P. Klemer, Y. Pei, and H. L. Graber, "Design and initial testing of system for simultaneous dynamic optical tomographic mammography," in *Biomedical Topical Meetings on CD-ROM*, Optical Society of America, Washington DC (2004).
16. P. He, M. Kaneko, M. Takai, K. Baba, Y. Yamashita, and K. Ohta, "Breast cancer diagnosis by laser transmission photoscanning with spectro-analysis," *Radiat. Med.* **8**, 1–15 (1990).
17. J. P. Culver, R. Choe, M. J. Holboke, L. Zubkov, T. Durduran, A. Slemple, V. Ntziachristos, B. Chance, and A. G. Yodanis, "Three-dimensional diffuse optical tomography in the parallel plane transmission geometry: Evaluation of a hybrid frequency domain/continuous wave clinical system for breast imaging," *Med. Phys.* **30**, 235–247 (2003).
18. M. Kaschke, H. Jess, G. Gaida, J. Kaltenbach, and W. Wrobel, "Transillumination imaging of tissue by phase modulation techniques," in *Advances in Optical Imaging and Photon Migration*, OSA Proceedings Series **24**, 88–92 (1994).
19. B. W. Pogue, M. Testorf, T. McBride, U. Osterberg, and K. Paulsen, "Instrumentation and design of a frequency-domain diffuse optical tomography imager for breast cancer detection," *Opt. Express* **1**, 391–403 (1997).
20. D. Grosenick, H. Wabnitz, H. H. Rinneberg, K. T. Moesta, and P. M. Schlag, "Development of a time-domain optical mammograph and first *in vivo* applications," *Appl. Opt.* **38**, 2927–2943 (1999).
21. M. A. Francheschini, K. T. Moesta, S. Fantini, G. Gaida, E. Gratton, H. Jess, W. W. Mantulin, M. Seeber, P. M. Schlag, and M. Kaschke, "Frequency-domain techniques enhance optical mammography: initial clinical results," *Proc. Natl. Acad. Sci. U.S.A.* **94**, 6468–6473 (1997).
22. F. E. W. Schmidt, M. E. Fry, E. M. C. Hillman, J. C. Hebden, and D. T. Delpy, "A 32-channel time-resolved instrument for medical optical tomography," *Rev. Sci. Instrum.* **71**, 256–265 (2000).
23. S. R. Arridge and W. R. B. Lionheart, "Nonuniqueness in diffusion-based optical tomography," *Opt. Lett.* **23**, 882–884 (1998).
24. D. Grosenick, H. Wabnitz, K. T. Moesta, J. Mucke, M. Möller, C. Stroszczynski, J. Stöbel, B. Wassermann, P. M. Schlag, and H. H. Rinneberg, "Concentration and oxygen saturation of haemoglobin of 50 breast tumours determined by time-domain optical mammography," *Phys. Med. Biol.* **49**, 1165–1181 (2004).
25. P. Taroni, G. Danesini, A. Torricelli, A. Pifferi, L. Spinelli, and R. Cubeddu, "Clinical trial of time-resolved scanning optical mammography at 4 wavelengths between 683 and 975 nm," *J. Biomed. Opt.* **9**, 464–473 (2004).
26. N. Morris, J. C. Hebden, T. D. Bland, and B. Balmer, "Role of patient feedback in the design and implementation of clinical trials of optical tomography of the breast," *Proc. SPIE* **5138**, 12–22 (2003).
27. B. W. Pogue, S. Jiang, H. Dehghani, C. Kogel, S. Soho, S. Srinivasan, X. Song, T. D. Tosteson, S. P. Poplack, and K. D. Paulsen, "Characterization of haemoglobin, water, and NIR scattering in breast tissue: analysis of intersubject variability and menstrual cycle

- changes," *J. Biomed. Opt.* **9**, 541–552 (2004).
28. S. B. Colak, D. G. Papaioannou, G. W. 't Hooft, M. B. Mark, H. Schomberg, J. C. J. Paasschens, J. B. M. Melissen, and N. Asten, "Tomographic image reconstruction from optical projections in light-diffusing media," *Appl. Opt.* **36**, 180–213 (1997).
 29. J. C. Hebden, T. D. Yates, A. Gibson, N. Everdell, S. R. Arridge, D. W. Chicken, M. Douek, and M. R. S. Keshtgar, "Monitoring recovery after laser surgery of the breast with optical tomography: a case study," *Appl. Opt.* **44**, 1898–1904 (2005).
 30. T. D. Yates, J. C. Hebden, A. Gibson, N. Everdell, S. R. Arridge, and M. Douek, "Optical tomography of the breast using a multi-channel time-resolved imager," *Phys. Med. Biol.* **50**, 2503–2517 (2005).
 31. J. C. Hebden, F. M. Gonzalez, A. P. Gibson, E. M. C. Hillman, R. Md. Yusof, N. Everdell, D. T. Delpy, G. Zaccanti, and F. Martelli, "Assessment of an in situ temporal calibration method for time-resolved optical tomography," *J. Biomed. Opt.* **8**, 87–92 (2003).
 32. E. M. C. Hillman, J. C. Hebden, F. E. W. Schmidt, S. R. Arridge, M. Schweiger, H. Dehghani, and D. T. Delpy, "Calibration techniques and datatype extraction for time-resolved optical tomography," *Rev. Sci. Instrum.* **71**, 3415–3427 (2000).
 33. M. Firbank, M. Oda, and D. T. Delpy, "An improved design for a stable and reproducible phantom material for use in near-infrared spectroscopy and imaging," *Phys. Med. Biol.* **40**, 955–960 (1995).
 34. I. Driver, J. W. Feather, P. R. King, and J. B. Dawson, "The optical properties of aqueous suspensions of Intralipid, a fat emulsion," *Phys. Med. Biol.* **34**, 1927–1930 (1989).
 35. T. Durduran, R. Choe, J. P. Culver, L. Zubkov, M. J. Holboke, J. Giammarco, B. Chance, and A. G. Yodh, "Bulk optical properties of healthy female breast tissue," *Phys. Med. Biol.* **47**, 2847–2861 (2002).
 36. A. Cerussi, F. Bevilacqua, N. Shah, D. Jakubowski, J. Butler, R. F. Holcombe, and B. J. Tromberg, "Sources of absorption and scattering contrast for near-infrared optical mammography," *Acad. Radiol.* **8**, 211–218 (2001).
 37. J. C. Hebden, H. Veenstra, H. Dehghani, E. M. Hillman, M. Schweiger, S. R. Arridge, and D. T. Delpy, "Three-dimensional time-resolved optical tomography of a conical breast phantom," *Appl. Opt.* **40**, 3278–3287 (2001).
 38. T. D. Yates, "Optical tomography for the detection and specification of breast disease," PhD Thesis, University of London (2005).
 39. H. Dehghani, B. Brooksby, K. Vishwanath, B. W. Pogue, and K. D. Paulsen, "The effects of internal refractive index variation in near-infrared optical tomography: a finite element modelling approach," *Phys. Med. Biol.* **48**, 2713–2728 (2003).
 40. S. R. Arridge, J. C. Hebden, M. Schweiger, F. E. W. Schmidt, M. E. Fry, E. M. C. Hillman, H. Dehghani, and D. T. Delpy, "A method for 3D time-resolved optical tomography," *Int. J. Imaging Syst. Technol.* **11**, 2–11 (2000).
 41. J. Schöberl, "NETGEN—An advancing front 2D/3D-mesh generator based on abstract rules," *Comput. Visual. Sci.* **1**, 41–52 (1997).
 42. A. E. Cerussi, D. Jakubowski, N. Shah, F. Bevilacqua, R. Lanning, A. J. Berger, D. Hsiang, J. Butler, R. F. Holcombe, and B. J. Tromberg, "Spectroscopy enhances the information content of optical mammography," *J. Biomed. Opt.* **7**, 60–71 (2002).
 43. S. R. Arridge, "Photon-measurement density-functions I: Analytical forms," *Appl. Opt.* **34**, 7395–7409 (1995).
 44. N. Shah, A. E. Cerussi, D. Jakubowski, D. Hsiang, J. Butler, and B. J. Tromberg, "Spatial variations in optical and physiological properties of healthy breast tissue," *J. Biomed. Opt.* **9**, 534–540 (2004).